

Boolean logic gate design principles in unconventional computers: an NMR case study

MATTHIAS BECHMANN^{1*}, ANGELIKA SEBALD^{1†}, SUSAN STEPNEY^{2‡}

¹ *Department of Chemistry, University of York, YO10 5DD, York, UK*

² *Department of Computer Science, University of York, YO10 5DD, York, UK*

Received 5 September 2011

We present a general method for analysing novel computational substrates to determine which of their parameters can be manipulated to exhibit the complete set of 2-input boolean logical operations. We demonstrate this approach with an NMR-based case study, showing which NMR parameters can be used to perform boolean logic.

Key words: NMR, boolean logic, canalising functions, universal gates, spin

1 INTRODUCTION

There is much work on *in materio* computing: exploiting unconventional material substrates and their dynamical properties to perform computation, and examining their computational properties and abilities. One of the more advanced is optical computing [33, 34]. Other, more exotic, substrates include nuclear spins in NMR experiments [16, 17, 24, 6], liquid crystals [12, 13, 14], conductive media [21, 22], reaction-diffusion chemical systems [19, 23, 27, 32], DNA [3, 4], and even slime moulds [2, 31].

The aim is to allow the material to do what comes naturally, under control of physical laws, and to exploit this natural dynamics as an efficient form of

* email: matthias.bechmann@york.ac.uk

† email: angelika.sebald@york.ac.uk

‡ email: susan@cs.york.ac.uk

class	members
0	T, F
1	A , NOT A , B , NOT B
2	A AND B ; A NAND B ; NOT A AND B , A AND NOT B , ...
3	A XOR B , NOT (A XOR B)

TABLE 1

The four equivalence classes of the 16 boolean 2-input logic gates. These correspond to equivalence classes under permutations of inputs and negation of the inputs and/or outputs [9], and to the different kinds of canalising functions [10].

computation [29, 30, 18]. The question arises: given some novel substrate, how to analyse its properties to determine whether it is a suitable medium for computation, and, if so, how it can be manipulated to perform computation in a manner best suited to that substrate.

Here we tackle a part of that problem: analysing a novel substrate to determine how it can be used to perform boolean logical operations. We present the design principles through a case study of using bulk nuclear spins, in the context of NMR (nuclear magnetic resonance) experiments.

2 THEORY AND BACKGROUND

2.1 Boolean functions and logic gates

The NAND and NOR logic gates are both *universal*, in that either can be used to construct all the other boolean 2-input logic gates. However, to do so, several such gates may be required. In an implementation, it is often more important to minimise the circuitry (the number of actual gates) than to minimise the number of types of gates.

Logic gates can be classified in terms of their symmetry properties [28, 11]. In terms of minimising circuitry, gates can be classified in terms of equivalence classes on permutations (rewiring) of inputs, and on negation of inputs and/or outputs (i.e. adding inverters, important in cases where they are significantly *cheaper* to implement than binary gates [9]). There are four such equivalence classes for the 16 boolean 2-input logic gates (Tables 1 and 2).

The same classification is found by considering canalising functions [10]. These are functions where the output is independent of one (or more) of the inputs, for one (or more) input values. Class 0 consists of the constant

A	B	T	B	$A \text{ NAND } B$	$A \text{ XOR } B$
0	0	1	0	1	0
0	1	1	1	1	1
1	0	1	0	1	1
1	1	1	1	0	0

TABLE 2

Truth tables of examples of the four classes of boolean logic gates, for each possible input value of A and B . Class 0 (example T) is independent of either input value. Class 1 (example B) is independent of one of the input values (here, A) for all possible inputs. Class 2 (example $A \text{ NAND } B$) is independent of one of the input values when the other has a particular value (here, it is independent of the value of B when A has the value 0). Class 3 (example $A \text{ XOR } B$) depends on both input values for all inputs.

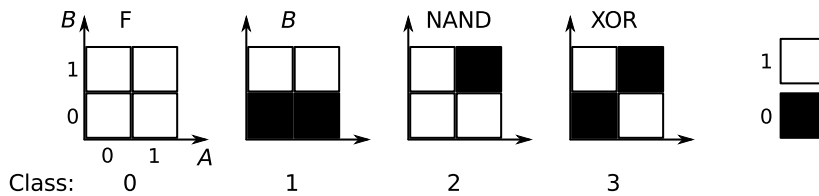


FIGURE 1

Logic-gates patterns and their different symmetries as visible from the two-dimensional representations of the canalising functions gate classes 0, 1, 2 and 3.

functions: the output is completely independent of the inputs. Class 1 consists of the strongly canalising functions: the output is independent of one of the inputs (for example, the function B is independent of the value of input A). Class 2 consists of the weakly canalising functions: the output is independent of one of the inputs when the other input has a specific value (for example, the function $A \text{ NAND } B$ is independent of the value of input B when the value of input A is false). Class 3 consists of the non-canalising functions: the output is determined by both inputs.

We use these symmetries/canalising properties of the gates (Figure 1) to look for analogous properties exhibited by the substrate that indicates a natural implementation route.

2.2 Nuclear spin dynamics

The most common application of NMR spectroscopy is that as a tool for structure elucidation of condensed matter in general, and of molecules in the liquid state in particular. The quantised nature of nuclear spin can also be assigned to the notion of a qubit in quantum computations [26]. Nuclear spins have also been used as a substrate to implement classical computation paradigms such as binary or continuous logic gates and circuits [24, 6].

A major reason for these computational applications to choose nuclear magnetic spins as the implementation platform is the rigour by which nuclear spin dynamics are described by quantum mechanics. In addition, the accuracy by which the macroscopically measured signal in an NMR experiment can be related to the underlying microscopic spin dynamics, using a density matrix approach, is nearly unrivalled by any other spectroscopic technique. In order to develop the formal relationship between the properties of logic gates and the quantum mechanical expressions describing the spin dynamics in a NMR experiment, we give a short summary of the necessary formalisms. For more details see textbooks on NMR [20]. Here we consider only uncoupled spins $S = 1/2$ in the liquid state.

The time evolution of an initial spin state vector $|\psi(t_a)\rangle$ is described as

$$|\psi(t)\rangle = \mathcal{U}(t, t_a) |\psi(t_a)\rangle \quad (1)$$

where $\mathcal{U}(t, t_a)$ is the time propagator describing the spin dynamics at every given point in time. The general orientation of the spin vector $|\psi\rangle$ is [20]

$$|\psi\rangle = \begin{pmatrix} \cos \frac{\theta_s}{2} e^{-i\frac{1}{2}\phi_s} \\ \sin \frac{\theta_s}{2} e^{+i\frac{1}{2}\phi_s} \end{pmatrix} \quad (2)$$

where θ_s and ϕ_s are the polar and azimuth angles. Its three-dimensional representation is given by

$$\begin{pmatrix} \langle \psi | I_x | \psi \rangle \\ \langle \psi | I_y | \psi \rangle \\ \langle \psi | I_z | \psi \rangle \end{pmatrix} = \frac{1}{2} \begin{pmatrix} \sin \theta_s \cos \phi_s \\ \sin \theta_s \sin \phi_s \\ \cos \theta_s \end{pmatrix} \quad (3)$$

describing a general Cartesian vector orientation (see Figure 2), where I_x , I_y and I_z are basis spin operators [25].

The time propagation of the macroscopic NMR signal is described by the density matrix $\rho(t) = |\psi(t)\rangle \langle \psi(t)|$ as

$$\rho(t) = \mathcal{U}(t, t_a) \rho(t_a) \mathcal{U}^\dagger(t, t_a) \quad (4)$$

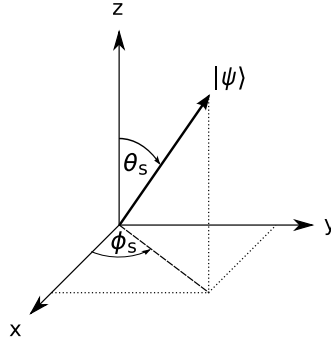


FIGURE 2
Spin state vector orientation of $|\psi\rangle$ in its Cartesian representation

where the bar signals the ensemble average. The thermal equilibrium density matrix is [20]

$$\rho_z^{\text{eq}} = \frac{1}{2} \mathbb{1} + \frac{1}{2} \lambda_B I_z \quad (5)$$

where $\lambda_B = \hbar\gamma B_0 / (k_B T)$ defines a Boltzmann factor, scaling the separation of spin energy levels, that can be interpreted as a spin polarisation along the z -axis.

The NMR system Hamiltonian and generator of the time evolution propagators for isolated, uncoupled spins is

$$\mathcal{H} = \mathcal{H}_{\text{CS}} + \mathcal{H}_{\text{rf}} \quad (6)$$

where \mathcal{H}_{CS} and \mathcal{H}_{rf} are the chemical shielding and radio frequency (r.f.) Hamiltonian, respectively. The explicit representation of the r.f. Hamiltonian is particularly simple in the rotating reference frame (RRF) as

$$\mathcal{H}_{\text{rf}} = \omega_p I_z + \kappa_p (I_x \cos \phi_p + I_y \sin \phi_p) \quad (7)$$

where ω_p is a frequency offset (relative to the frequency of RRF), and κ_p and ϕ_p are the amplitude and phase of the pulse. Figure 3(a) summarises the behaviour of the magnetisation vector M (Eqs. (1)–(23)) under the influence of a r.f. pulse; Figure 3(b) depicts the relevant parameters. Pulses applied to spins resonating at the rotation frequency of the RRF are described by the system Hamiltonian

$$\mathcal{H} = \mathcal{H}_{\text{rf}} = \kappa_p (I_x \cos \phi_p + I_y \sin \phi_p) \quad (8)$$

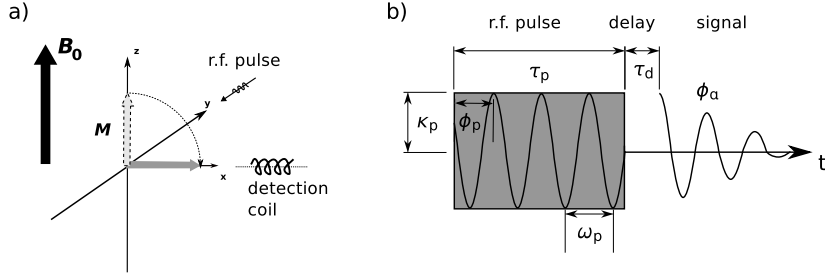


FIGURE 3

NMR single-pulse experiment: (a) rotation of the magnetisation vector \mathbf{M} by a r.f. pulse $R_{\phi_p}(\beta)$ with $\phi_p = \frac{\pi}{2}$ and $\beta = \kappa_p \tau_p = \frac{\pi}{2}$; (b) the relevant parameters describing the single-pulse NMR experiment (pulse amplitude κ_p , pulse duration τ_p , pulse phase ϕ_p , pulse frequency ω_p , free evolution delay τ_d and acquisition phase ϕ_a).

and the overall system Hamiltonian for uncoupled isolated spins $S = 1/2$ is

$$\begin{aligned} \mathcal{H} &= \mathcal{H}_{CS} + \mathcal{H}_{rf} : \text{during pulse} \\ \mathcal{H} &= \mathcal{H}_{CS} : \text{during free evolution} \end{aligned} \quad (9)$$

including a chemical shielding offset \mathcal{H}_{CS} from the RRF frequency.

The general form of the time evolution propagator in NMR is

$$\mathcal{U}(t_b, t_a) = \mathcal{T} \exp \left\{ -i \int_{t_a}^{t_b} \mathcal{H}(t) dt \right\} \quad (10)$$

where \mathcal{T} is the Dyson time-ordering operator [25].

Dependent on the symmetry of the Hamiltonian, different (simpler) expressions for the propagator can be formulated

$$\mathcal{H}(t) = \mathcal{H} \rightarrow \mathcal{U}(t_b, t_a) = \exp \{ -i \mathcal{H} (t_b - t_a) \} \quad (11)$$

time independent

$$[\mathcal{H}(t'), \mathcal{H}(t'')] = 0 \rightarrow \mathcal{U}(t_b, t_a) = \exp \{ -i \int_{t_a}^{t_b} dt' \mathcal{H}(t') \} \quad (12)$$

self – commuting

$$\mathcal{H}(t_a + \tau) = -\mathcal{H}(t_b - \tau) \rightarrow \mathcal{U}(t_b, t_a) = 1 ; \text{anti-symmetric} \quad (13)$$

$$\mathcal{U}(t_b, t_a) = \pm 1 ; \text{cyclic} \quad (14)$$

In the case of a hard pulse, a so-called δ pulse is usually a valid description

of the time propagator

$$\begin{aligned}
\mathcal{U}(t_b, t_a) &= \exp\{-i\mathcal{H}_{\text{rf}}\tau_p\}; \tau_p = t_b - t_a \\
&= \exp\{-i\kappa_p\tau_p(I_x \cos\phi_p + I_y \sin\phi_p)\} \\
&= R_{\phi_p}(\beta); \beta = \kappa_p\tau_p
\end{aligned} \tag{15}$$

which is equivalent to the rotation operation $R_{\phi_p}(\beta)$. It generates a rotation by an angle β about an axis in the xy -plane with azimuth angle ϕ_p . For a sequence of δ pulses the propagator can be factorised as

$$\begin{aligned}
\mathcal{U}(t_c, t_a) &= \mathcal{U}_2(t_c, t_b)\mathcal{U}_1(t_b, t_a); \tau_{p1} = t_b - t_a \text{ and } \tau_{p2} = t_c - t_b \\
&= R_{\phi_{p2}}(\beta_2)R_{\phi_{p1}}(\beta_1); \beta_1 = \kappa_{p1}\tau_{p1}; \beta_2 = \kappa_{p2}\tau_{p2}
\end{aligned} \tag{16}$$

The explicit form of these propagators is equivalent to rotation operators in two dimensions and is [20]

$$R_x(\beta) = e^{-i\beta I_x} = \begin{pmatrix} \cos\frac{\beta}{2} & -i\sin\frac{\beta}{2} \\ -i\sin\frac{\beta}{2} & \cos\frac{\beta}{2} \end{pmatrix} \tag{17}$$

$$R_y(\beta) = e^{-i\beta I_y} = \begin{pmatrix} \cos\frac{\beta}{2} & -\sin\frac{\beta}{2} \\ \sin\frac{\beta}{2} & \cos\frac{\beta}{2} \end{pmatrix} \tag{18}$$

$$R_z(\beta) = e^{-i\beta I_z} = \begin{pmatrix} e^{-i\frac{\beta}{2}} & 0 \\ 0 & e^{+i\frac{\beta}{2}} \end{pmatrix} \tag{19}$$

$$\begin{aligned}
R_\phi(\beta) &= e^{-i\beta(I_x \cos\phi + I_y \sin\phi)} = \begin{pmatrix} \cos\frac{\beta}{2} & -i\sin\frac{\beta}{2}e^{-i\phi} \\ -i\sin\frac{\beta}{2}e^{+i\phi} & \cos\frac{\beta}{2} \end{pmatrix} \\
&= R_z(\phi)R_x(\beta)R_z(-\phi)
\end{aligned} \tag{20}$$

After a pulse $R_{\phi_p}(\beta)$ with phase $\phi_p = \frac{\pi}{2}$ and flip angle $\beta = \frac{\pi}{2}$ the thermal equilibrium density matrix ρ_z^{eq} is transformed according to

$$\begin{aligned}
R_{\frac{\pi}{2}}\left(\frac{\pi}{2}\right)\rho_z^{\text{eq}}R_{\frac{\pi}{2}}^\dagger\left(\frac{\pi}{2}\right) &= \frac{1}{2}\mathbb{1} + \frac{\lambda_B}{2} \begin{pmatrix} 0 & 1 \\ 1 & 0 \end{pmatrix} \\
&= \frac{1}{2}\mathbb{1} + \frac{1}{2}\lambda_B I_x \\
&= \rho_x
\end{aligned} \tag{21}$$

yielding spin polarisation along the $+x$ direction.

A r.f. pulse $R_{\phi_p}(\beta)$ applied to an initial state $\rho^{(i)}$ generates a spin density matrix that can be expressed in terms of its final polar coordinates $\rho(\phi_s, \theta_s) =$

$|\psi\rangle\langle\psi|$ (Eq. (2)) or as a function of the pulse parameters rotating an initial state $\rho^{(i)}(\phi_p, \beta)$. For example when starting from $\rho^{(z)} = \rho_z^{\text{eq}}$ the final state is

$$\rho^{(z)}(\phi_p, \beta) = \frac{1}{2}\mathbb{1} + \frac{\lambda_B}{2} \begin{pmatrix} \cos\beta & -i\sin\beta e^{-i\phi_p} \\ -i\sin\beta e^{+i\phi_p} & -\cos\beta \end{pmatrix} \quad (22)$$

and the relation $\rho(\phi_s, \theta_s) = \rho^{(z)}(\phi_p, \beta)$ holds for $(\phi_s, \theta_s) = (\phi_p - \frac{\pi}{2}, \beta)$.

Equivalently to the calculation of the three-dimensional spin-vector orientation in Eq. (3) from the two-dimensional spin state $|\psi\rangle$ (Eq. (2)), the three-dimensional magnetisation vector \mathbf{M} can then be calculated from any given two-dimensional density matrix ρ as

$$\mathbf{M} = \begin{pmatrix} \overline{\langle I_x \rangle} \\ \overline{\langle I_y \rangle} \\ \overline{\langle I_z \rangle} \end{pmatrix} = \begin{pmatrix} \text{Tr}\{\rho I_x\} \\ \text{Tr}\{\rho I_y\} \\ \text{Tr}\{\rho I_z\} \end{pmatrix} \quad (23)$$

In the case of single isolated spins this also implies the equivalence in interpretation of the spin vector orientation in Figure 2 and the magnetisation vector \mathbf{M} .

In general a NMR pulse sequence can consist of any number and parametrisation of r.f. pulses and free evolution delays. This provides for numerous options for the implementation of e.g. logic gates. The most useful parametrisation in the following is the one describing the NMR signal as a function of the pulse sequence, $\rho^{(i)}(\phi_p, \beta)$.

3 LOGIC GATES FROM NMR PARAMETERS

3.1 Classification of NMR parameters

The most common parameters describing a NMR experiment, open for use as control parameters to implement logic operations, are $\{\kappa_p, \phi_p, \tau_p, \omega_p, \tau_d, \phi_a\}$: pulse amplitude, pulse phase, pulse duration, pulse frequency, free evolution delay, and receiver phase, respectively (see Figure 3).

A heuristic classification rule has been given elsewhere [24], separating logic gates based on the relation between the experimental NMR parameters chosen:

1. if the effect of the first parameter cannot be compensated for by setting the second parameter (canalising input value), then AND, >, < NOR, OR, \leq , \geq , NAND gates can be constructed (asymmetric gates);

class	canalising input values for fixed:	A	B
0	T	2	2
1	B	0	2
2	$A \text{ NAND } B$	1	1
3	$A \text{ XOR } B$	0	0

TABLE 3

Number of canalising input values for the four gate classes. Demonstrated for one representative member of every class: T, B , $A \text{ NAND } B$, $A \text{ XOR } B$. The respective truth tables for these four gates are shown in Table 2.

2. if the effect of the first parameter can be compensated by a setting of the second parameter, then XOR and XNOR gates can be constructed (symmetric gates).

This classification of logic gates seamlessly integrates in a generalised description by using the concept of canalising functions [10] and equivalence classes [9]. Fixing one of the inputs of a logic gate (A or B) is a *canalising input value* if changing the other (unfixed) input does not alter the gate output. The number of all possible canalising input values for a given logic gate for all possible inputs states is used as a criterion to assign logic gates to one of four classes (see Table 3):

class 0 two canalising input values for either of the two inputs A and B

class 1 two canalising input values for exactly one of the inputs A or B

class 2 one canalising input values for either of the two inputs A and B

class 3 no canalising input values for either inputs A and B

These four classes also show unique symmetry patterns in their two-dimensional representations (see Figure 1). Rows and columns of equal coloured squares signal the presence of a canalising input. These patterns can be used to map functions $f(x1, x2)$ to corresponding canalising functions and, therefore, the logic gate(s) they can naturally implement are readily identified.

According to our previous definitions [24] a strong parameter would generate a canalising function for at least one of its states (class 0, 1 and 2), because altering the other parameter causes no change in the NMR output. On the other hand, for a weak parameter the output would always change (class 3).

In the following we demonstrate how the abstract concept of canalising functions relates to the symmetries and commutation relations of the NMR Hamiltonian, the time evolution propagator, and the experimental output of a NMR experiment.

3.2 Canalising input values in NMR context

Here we consider a system Hamiltonian that consists only of the \mathcal{H}_{rf} term. Hence, we are in the single spin, strong pulse, on-resonant regime, and for simplicity we only consider the experimental parameters $\kappa_{\text{p}}, \phi_{\text{p}}, \tau_{\text{p}}$ (r.f. pulse amplitude, phase and duration) for logic gate generation.

The NMR r.f. pulse propagator $R_{\phi_{\text{p}}}(\beta) = R_z(\phi_{\text{p}}) R_x(\beta) R_z(-\phi_{\text{p}})$ (Eq. (20)) is the general rotation operator about an axis in the traverse xy -plane of the RRF. It therefore commutes with a particular spin state ($I_{\phi_{\text{p}}}$) in the transverse plane for a given value ϕ_{p} (e.g. for $\phi_{\text{p}} = 0$; $[R_0(\beta), I_x] = 0$ independent of the value of β). However, $R_{\phi_{\text{p}}}(\beta)$ will never commute with the thermal equilibrium state $\rho_z^{\text{eq}} (\sim I_z)$ (Eq. (5)), which is perpendicular to the xy -plane. For example, a $R_0(\frac{\pi}{2})$ pulse applied to z -magnetisation ($\sim I_z$) will flip it to the $-y$ direction, and therefore change the spin state and its orientation. A subsequent pulse applied using $R_{-\frac{\pi}{2}}(\frac{\pi}{2})$ will leave it unaltered, since the system is in the $-I_y$ spin state, an eigenstate of $R_{-\frac{\pi}{2}}(\frac{\pi}{2})$ and, therefore, a canalising input is generated in this second step. One can postulate now that a *canalising input* is generated by an r.f. pulse if:

1. $R_{\phi_{\text{p}}}(\beta)$ leaves the system state unaltered (eigenstate; $[R_{\phi_{\text{p}}}(\beta), \rho] = 0$),
2. $R_{\phi_{\text{p}}}(\beta) = \mathbb{1}$, the unity operator.

In the following this behaviour and the possibility of generating canalising input values is analysed. First we consider single-pulse experiments assuming different initial system-state preparations $\rho^{(i)}$. Second we consider experiments composed of more than one pulse.

Single-pulse gates

The signal as detected during a NMR experiment is not the effect of the full spin magnetisation vector \mathbf{M} as given in Eq. (23) but only its projection into the xy -plane [20]. Hence, the physically meaningful quantities that can be measured by NMR are the magnetisation vector components $M_x = \overline{\langle I_x \rangle}$ and $M_y = \overline{\langle I_y \rangle}$, describing the orientational distribution of this projection, and the magnitude $M_{xy} = \sqrt{\langle I_x \rangle^2 + \langle I_y \rangle^2}$ describing the total amount of magnetisation present in the xy -plane. The functional structure of M_x, M_y

and M_{xy} is determined by the r.f. pulse $R_{\phi_p}(\beta)$ and the initial spin state $\rho^{(i)}$ to which the r.f. pulse is applied. M_x , M_y and M_{xy} are therefore functions of pulse phase ϕ_p , pulse flip angle $\beta = \kappa_p \tau_p$ and the initial direction of the spin magnetisation.

The spin magnetisation can assume every possible orientation, while the r.f. pulse and therefore the rotation axis of the spin magnetisation is restricted to the xy -plane. It is instructive to examine scenarios where the initial spin state $\rho^{(i)}$ is either perpendicular to the xy -plane and never commutes with the r.f. pulse operator $R_{\phi_p}(\beta)$, or where it is coplanar to it and therefore can commute.

Starting from thermal equilibrium state The most simple and natural initial spin state is the one the system assumes at thermal equilibrium $\rho^{(i)} = \rho_z^{\text{eq}}$ (Eq. (5)). Here the spin polarisation is pointing along the z -axis, perpendicular to the xy -plane and $R_{\phi_p}(\beta)$ never commutes with it. ρ_z^{eq} transforms under the influence of a pulse $R_{\phi_p}(\beta)$ as

$$\rho^{(z)}(\phi_p, \beta) = R_{\phi_p}(\beta) \rho_z^{\text{eq}} R_{\phi_p}^\dagger(\beta) \quad (24)$$

After this single pulse the spin magnetisation vector \mathbf{M} (Eq. (23)) is a function of pulse flip angle β and pulse phase ϕ_p

$$\begin{pmatrix} M_x \\ M_y \\ M_z \end{pmatrix} = \begin{pmatrix} \text{Tr} \{ \rho^{(z)}(\phi_p, \beta) I_x \} \\ \text{Tr} \{ \rho^{(z)}(\phi_p, \beta) I_y \} \\ \text{Tr} \{ \rho^{(z)}(\phi_p, \beta) I_z \} \end{pmatrix} = \frac{\lambda_B}{4} \begin{pmatrix} \sin \phi_p \sin \beta \\ -\cos \phi_p \sin \beta \\ \cos \beta \end{pmatrix} \quad (25)$$

and the NMR measurable quantities $M_x(\phi_p, \beta)$, $M_y(\phi_p, \beta)$ and $M_{xy}(\phi_p, \beta) = \frac{\lambda_B}{4} |\sin \beta|$ are readily determined. These quantities are functions of the two pulse parameters ϕ_p and β just like the binary logic gates are functions of the two inputs A and B (Table 2). An instructive way to analyse $M_x(\phi_p, \beta)$, $M_y(\phi_p, \beta)$ and $M_{xy}(\phi_p, \beta)$, as to which logic gates can be implemented by them, is by examining their representation as two-dimensional contour plots. These are shown in Figure 4. A comparison with the two-dimensional sketches of 2-input logic gates in Figure 1 immediately reveals agreements and disagreements in symmetries.

In principle the functions $M_x(\phi_p, \beta)$, $M_y(\phi_p, \beta)$ and $M_{xy}(\phi_p, \beta)$ are continuous in ϕ_p and β whereas logic gates are boolean functions of A and B that can only assume the discrete values of $\{0, 1\}$. In order to map the continuous functions in Figure 4 to the four possible discrete sets (A, B) of a logic gate one has to find four discrete pairs (ϕ_p, β) at which to evaluate the

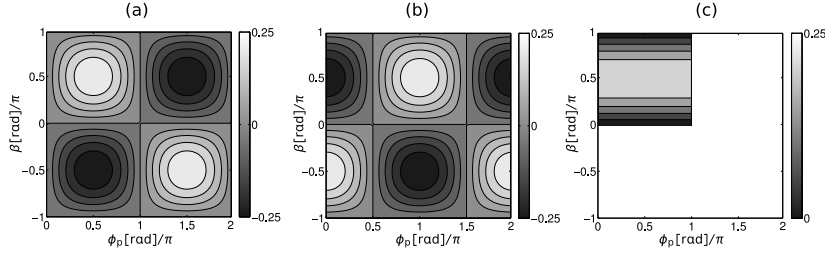


FIGURE 4

Contour plots of the NMR detectable quantities (a) $M_x = \overline{\langle I_x \rangle}$, (b) $M_y = \overline{\langle I_y \rangle}$ and (c) $M_{xy} = \sqrt{\overline{\langle I_x \rangle}^2 + \overline{\langle I_y \rangle}^2}$ (Eq. (25)) as a function of the pulse parameters ϕ_p and β . The initial spin polarisation has been along the z -axis (ρ_z^{eq}) and $\lambda_B = 1$ has been assumed. The ranges for ϕ_p and β have been chosen such that the only symmetry operation necessary to generate a full, infinite plot are horizontal and vertical translations.

continuous functions and where the symmetry pattern of the desired logic gate results.

For example from Figure 4(a) depicting M_x , one can directly identify the symmetry pattern corresponding to a class 3 gate in Figure 1. In order to implement the class 3 (XOR) gate (Table 2) one needs to define four discrete value sets ($\phi_p = \phi_p^A, \beta = \beta^B$) (with $A, B \in \{0, 1\}$). Inspection of Figure 4(a) immediately suggests the positive and negative extrema as possible candidates: Selecting the pair $(\phi_p^{A=0}, \beta^{B=0}) = (\frac{\pi}{2}, -\frac{\pi}{2})$ the detected output is $M_x(\phi_p^{A=0} = \frac{\pi}{2}, \beta^{B=0} = -\frac{\pi}{2}) = -0.25$. In the same fashion, $M_x(\frac{\pi}{2}, \frac{\pi}{2}) = 0.25$, $M_x(\frac{3\pi}{2}, -\frac{\pi}{2}) = 0.25$ and $M_x(\frac{3\pi}{2}, \frac{\pi}{2}) = -0.25$ are calculated for the remaining XOR gate input configurations. The values of $M_x(\phi_p, \beta)$, $M_y(\phi_p, \beta)$ and $M_{xy}(\phi_p, \beta)$ in Figure 4 are calculated assuming $\lambda_B = 1$. Mapping these values to the final boolean values $\{0, 1\}$ is achieved by scaling them by a factor of 4.

A class 3 gate is characterised by the absence of any canalising input (Table 3). A change in ϕ_p^A or β^B will therefore always change the value $M_x(\phi_p^A, \beta^B)$. In order to change one of the parameters ϕ_p^A or β^B and achieve the same result in $M_x(\phi_p^A, \beta^B)$ one can take advantage of the periodicity of the trigonometric functions in Eq. (25) and in this way $M_x(\frac{\pi}{2}, -\frac{\pi}{2}) = M_x(\frac{5\pi}{2}, -\frac{\pi}{2}) = -0.25$ and $M_x(\frac{\pi}{2}, \frac{\pi}{2}) = M_x(\frac{5\pi}{2}, \frac{\pi}{2}) = 0.25$ can be implemented. This gate is evaluating ϕ_p^A at values separated by 2π and the

class	ϕ_p^A		β^B		Output= $M_x(\phi_p^A, \beta^B)$				gate
	0	1	0	1	00	01	10	11	
0	$\frac{\pi}{2}$	$\frac{5\pi}{2}$	$\frac{\pi}{2}$	$\frac{5\pi}{2}$	0.25	0.25	0.25	0.25	T
1	$\frac{\pi}{2}$	$\frac{5\pi}{2}$	$-\frac{\pi}{2}$	$\frac{\pi}{2}$	-0.25	0.25	-0.25	0.25	B
2	π	$\frac{3\pi}{2}$	0	$\frac{\pi}{2}$	0	0	0	-0.25	A NAND B
3	$\frac{\pi}{2}$	$\frac{3\pi}{2}$	$-\frac{\pi}{2}$	$\frac{\pi}{2}$	-0.25	0.25	0.25	-0.25	A XOR B

TABLE 4

Some selected values ϕ_p and β to generate one representative gate of every gate class using $M_x(\phi_p, \beta)$ as shown in Figure 4(a).

gate is therefore independent of a change in ϕ_p^A no matter which of its two permitted values β^B assumes. A change in β^B , however, will always change $M_x(\phi_p^A, \beta^B)$. This behaviour corresponds to a class 1 gate with two canalising input values for one parameter. In order to implement class 2 gates a comparison of the logic gate patterns and the contour plot for $M_x(\phi_p^A, \beta^B)$ suggests a restriction of the parameter range to smaller intervals. For example, one may choose the interval $\phi_p \in [\pi, \frac{3\pi}{2}]$ and $\beta \in [0, \frac{\pi}{2}]$ to implement a NAND gate representing a class 2 (NAND) gate (see Table 4). The implementation of a class 0 gate requires two canalising input values for both ϕ_p^A and β^B . As in the class 1 (B) gate scenario the periodicity of $M_x(\phi_p^A, \beta^B)$ can be used to achieve canalising inputs. However, this time both parameters have to undergo the 2π value changes. Alternatively one can use pulses corresponding to rotation operators $R_{\phi_p}(\beta) = \pm \mathbb{1}$ for generating canalising inputs for any parameter configuration of ϕ_p^A or β^B .

Having demonstrated how to implement one member of every gate class it is now a trivial task to generate implementations of all the members of a given gate class. By using the symmetry operations of permuting the input assignment of A and B to ϕ_p and β , inverting the input or the output, the remaining gates are obtained directly.

This shows that all 2-input logic gates can be implemented using the functions $M_x(\phi_p, \beta)$. $M_x(\phi_p, \beta)$ and $M_y(\phi_p, \beta)$ are both products of two linear trigonometric functions, differing only by a phase shift of $\frac{\pi}{2}$ in the factor depending on ϕ_p ($\sin(\phi_p + \frac{\pi}{2}) = \cos \phi_p$). This phase shift can be seen in Figure 4(a) and (b) as a horizontal shift by $\frac{\pi}{2}$, otherwise both plots are identical. Their overall symmetry pattern is that of a class 3 gate. Hence, everything said

about $M_x(\phi_p, \beta)$ implementations equally holds for $M_y(\phi_p, \beta)$.

However the same can not be said about the magnetisation magnitude $M_{xy}(\phi_p, \beta)$ (Figure 4(c)). $M_{xy}(\phi_p, \beta) = M_{xy}(\beta) = \frac{\lambda_B}{4} |\sin \beta|$ is only a function of the pulse flip angle β and, therefore, displays a contour plot with a symmetry corresponding to a class 1 gate.

The behaviour of the functions under permutation of the variables ϕ_p and β and/or their inversion distinguishes $M_x(\phi_p, \beta)$, $M_y(\phi_p, \beta)$ and $M_{xy}(\phi_p, \beta)$ from each other. $M_x(\phi_p, \beta)$ is invariant to permutation of the variables while $M_{xy}(\phi_p, \beta)$ is not. In contrast, $M_x(\phi_p, \beta)$ changes under inversion of its variables $\phi_p \rightarrow -\phi_p$ or $\beta \rightarrow -\beta$, while $M_{xy}(\phi_p, \beta)$ is invariant to inversion of $\phi_p \rightarrow -\phi_p$. $M_y(\phi_p, \beta)$ shows the same behaviour as $M_{xy}(\phi_p, \beta)$ under these transformations. However, a simple shift in $\phi_p = \frac{\pi}{2}$ gives $M_x(\phi_p, \beta) = M_y(\phi_p + \frac{\pi}{2}, \beta)$, an operation which is not possible for $M_{xy}(\phi_p, \beta)$ since it is independent of ϕ_p . The differences in behaviour arise because for $M_x(\phi_p, \beta)$ and $M_y(\phi_p, \beta)$ both variables ϕ_p and β are arguments of products of trigonometric functions, which generates function values in the range of $[-1, 1]$, whereas $M_{xy}(\phi_p, \beta)$ has trigonometric function values in $[-1, 1]$ only for the variable β .

In principle, the task of implementing all 2-input logic gates by NMR spectroscopy is already accomplished by using only the simplest of all NMR experiments: starting from thermal equilibrium and only using a single r.f. pulse. This scenario can therefore serve as a Universal Logic Module (ULM) [35]. There are, however, good reasons why one needs to explore other starting conditions, and more complicated NMR pulse sequences. NMR is uniquely suitable as a single testbed for the implementation of classical as well as quantum computations. In common formulations of quantum algorithms the initial state of the computation is not the thermal equilibrium state but a superposition state [16]. For valid comparisons between classical and quantum algorithm NMR implementations the same initial (superposition) state should be used. Further, it may be desirable to construct more extended circuitry than just a single logic gate [15]. Then gate implementations that can deal with initial states other than ρ_z^{eq} are attractive as an efficient means of taking advantage of the output of a logic gate without having to restore the initial state ρ_z^{eq} before the next logic gate in a circuit can be executed.

Starting from superposition state A r.f. pulse $R_{\frac{\pi}{2}}(\frac{\pi}{2})$ applied to ρ_z^{eq} generates the superposition state $\rho_x = \frac{1}{2} \mathbb{1} + \frac{1}{2} \lambda_B I_x$, which corresponds to spin polarisation pointing along the $+x$ -axis. Here we take ρ_x as the initial super-

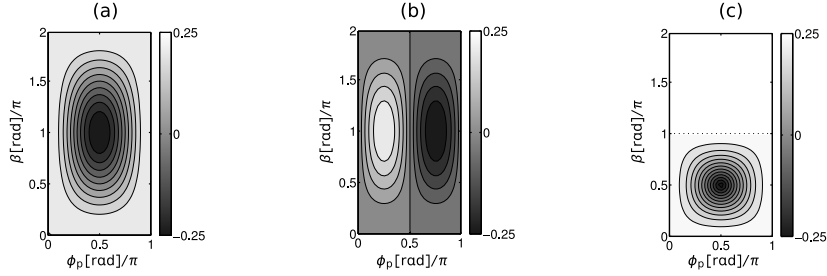


FIGURE 5

Contour plots of the NMR detectable quantities (a) $M_x = \overline{\langle I_x \rangle}$, (b) $M_y = \overline{\langle I_y \rangle}$ and (c) $M_{xy} = \sqrt{\overline{\langle I_x \rangle^2} + \overline{\langle I_y \rangle^2}}$ (Eq. (28)) as a function of the pulse parameters ϕ_p and β . The initial spin polarisation has been along the x -axis (ρ_x) and $\lambda_B = 1$ has been assumed. The ranges for ϕ_p and β have been chosen such that the only symmetry operation necessary to generate a full, infinite plot are horizontal and vertical translations.

position state. The commutator between $R_{\phi_p}(\beta)$ and ρ_x is

$$[R_{\phi_p}(\beta), \rho_x] = -\lambda_B I_z \sin \phi_p \sin \frac{\beta}{2} \quad (26)$$

and is zero for values $\phi_p = n\pi$. These angles correspond to rotations around the positive and negative x -axis (the commutator is also zero for $\beta = 2n\pi$, but these angles represent trivial 2π rotations). ρ_x transforms under the influence of a r.f. pulse $R_{\phi_p}(\beta)$ as

$$\rho^{(x)}(\phi_p, \beta) = R_{\phi_p}(\beta) \rho_x R_{\phi_p}^\dagger(\beta) \quad (27)$$

The r.f. pulse generates a magnetisation vector \mathbf{M} (Eq. (23)) as a function of pulse flip angle β and pulse phase ϕ_p according to

$$\begin{pmatrix} M_x \\ M_y \\ M_z \end{pmatrix} = \begin{pmatrix} \text{Tr} \{ \rho^{(x)}(\phi_p, \beta) I_x \} \\ \text{Tr} \{ \rho^{(x)}(\phi_p, \beta) I_y \} \\ \text{Tr} \{ \rho^{(x)}(\phi_p, \beta) I_z \} \end{pmatrix} = \frac{\lambda_B}{4} \begin{pmatrix} 1 - 2 \sin^2 \phi_p \sin^2 \frac{\beta}{2} \\ \sin 2\phi_p \sin^2 \frac{\beta}{2} \\ -\sin \phi_p \sin \beta \end{pmatrix} \quad (28)$$

All the quantities $M_x(\phi_p, \beta)$, $M_y(\phi_p, \beta)$ and

$M_{xy}(\phi_p, \beta) = \frac{\lambda_B}{4} \sqrt{1 - \sin^2 \phi_p \sin^2 \beta}$ are functions of ϕ_p and β . Contour plots of these three functions are shown in Figure 5. Again, agreements and disagreements in symmetries are found by comparison with Figure 1. Inspection of Figures 4 and 5 immediately reveals differences in the transformation behaviour of ρ_x and ρ_z^{eq} .

As shown earlier it is possible to implement any logic gate from a NMR measurable quantity that has the symmetry of a class 3 gate in Figure 1 (e.g. $M_x(\phi_p, \beta)$ in Figure 4(a)). However, none of the three contour plots in Figure 5 displays this symmetry and no class 3 gates can be implemented. The symmetries present belong to those of class 0, 1 and 2 gates and can be found in any of the three contour plots. Implementing class 1 gates requires taking advantage of the periodicity of the functions $M_x(\phi_p, \beta)$, $M_y(\phi_p, \beta)$ and $M_{xy}(\phi_p, \beta)$ in order to generate canalising inputs. Class 2 gates use a reduced parameter range for ϕ_p and β .

Permutation of ϕ_p and β changes $M_x(\phi_p, \beta)$, $M_y(\phi_p, \beta)$, while $M_{xy}(\phi_p, \beta)$ stays invariant under this operation. $M_x(\phi_p, \beta)$ and $M_{xy}(\phi_p, \beta)$ are invariant under input inversion $\phi_p \rightarrow -\phi_p$ or $\beta \rightarrow -\beta$ while $M_y(\phi_p, \beta)$ is only invariant under $\beta \rightarrow -\beta$. All functions are now periodic with π in ϕ_p because of their dependence on $\sin^2 \phi_p$ or $\sin 2\phi_p$. $M_x(\phi_p, \beta)$ and $M_y(\phi_p, \beta)$ have a 2π periodicity interval in β and π periodicity for $M_{xy}(\phi_p, \beta)$. All the functions $M_x(\phi_p, \beta)$, $M_y(\phi_p, \beta)$ and $M_{xy}(\phi_p, \beta)$ are the products of two trigonometric functions of which at least one is quadratic. The squaring reduces the trigonometric function values to the interval $[0, 1]$ and therefore, it is not possible to have a symmetry behaviour required for class 3 gates.

The rotation operator $R_{\phi_p}(\beta)$ *not commuting* with the initial density matrix ρ_z^{eq} leads to the functions $M_x(\phi_p, \beta)$, $M_y(\phi_p, \beta)$ and $M_{xy}(\phi_p, \beta)$ described by products of linear trigonometric functions and the ability to implement *all* logic gates. The rotation operator $R_{\phi_p}(\beta)$ *commuting* with the initial density matrix ρ_x , however, leads to the functions $M_x(\phi_p, \beta)$, $M_y(\phi_p, \beta)$ and $M_{xy}(\phi_p, \beta)$ characterised by quadratic trigonometric factors and *does not* permit the implementation of all logic gates. Achieving universality when starting from ρ_x therefore requires a different rotation operator that never commutes with ρ_x . This could be achieved by choosing different pairs of parameters from the set of parameters describing the single-pulse experiment (Figure 3) such that a non-commuting rotation operator for ρ_x results. Alternatively, one can keep the pair of parameters ϕ_p and β , and use more than one r.f. pulse, with rotation operators such as $R_{\phi_{p2}}(\beta_2) R_{\phi_{p1}}(\beta_1)$. This latter option we consider next.

Two-pulse gates

The initial density matrix ρ_x transforms under the influence of two r.f. pulses $R_{\phi_{p2}}(\beta_2) R_{\phi_{p1}}(\beta_1)$ as

$$\rho^{(x)}(\phi_{p2}, \beta_2, \phi_{p1}, \beta_1) = R_{\phi_{p2}}(\beta_2) R_{\phi_{p1}}(\beta_1) \rho_x R_{\phi_{p1}}^\dagger(\beta_1) R_{\phi_{p2}}^\dagger(\beta_2) \quad (29)$$

Thus, the NMR detectable quantities $M_x(\phi_{p2}, \beta_2, \phi_{p1}, \beta_1)$, $M_y(\phi_{p2}, \beta_2, \phi_{p1}, \beta_1)$ and $M_{xy}(\phi_{p2}, \beta_2, \phi_{p1}, \beta_1)$ are functions of the four variables ϕ_{p2} , β_2 , ϕ_{p1} and β_1 . Any two of these variables can serve as logic gate input parameters with the remaining two fixed. This offers a high degree of flexibility in assigning parameters as variable (and to control the logic gate), and as fixed.

A trivial example is based on the fact that all 2-input gates can be implemented when starting from thermal equilibrium magnetisation by a single pulse. Starting from ρ_x , a first r.f. pulse $R_{\frac{\pi}{2}}(-\frac{\pi}{2})$ generates ρ_z^{eq} and yields $\phi_{p1} = \frac{\pi}{2}$ and $\beta_1 = -\frac{\pi}{2}$. From there on any second r.f. pulse $R_{\phi_{p2}}(\beta_2)$ generates a functional behaviour identical to that of the single-pulse scenario in Eq. (25), generating universality.

Another strategy uses the commutation properties of the rotation operators. In the single-pulse scenario, starting from ρ_z^{eq} all logic gates can be implemented because the overall rotation operator never commutes with the initial density matrix. In the two-pulse scenario, $R_{\phi_{p2}}(\beta_2)R_{\phi_{p1}}(\beta_1)$ must not commute with ρ_x . This implies further that the first r.f. pulse $R_{\phi_{p1}}(\beta_1)$ must not commute with ρ_x , otherwise Eq. (29) simplifies to $\rho^{(x)}(\phi_{p2}, \beta_2) = R_{\phi_{p2}}(\beta_2)\rho_x R_{\phi_{p2}}^\dagger(\beta_2)$ (identical to Eq. (27)) which *can not* implement all logic gates. To avoid commutation, ϕ_{p1} should never be fixed to values $n\pi$ (Eq. (26)). The second r.f. pulse $R_{\phi_{p2}}(\beta_2)$ must not commute with the spin basis operators I_x or I_y when calculating $M_x(\phi_{p2}, \beta_2, \phi_{p1}, \beta_1) = \overline{\langle I_x \rangle}$ or $M_y(\phi_{p2}, \beta_2, \phi_{p1}, \beta_1) = \overline{\langle I_y \rangle}$ (Eq. (23)), otherwise $R_{\phi_{p2}}(\beta_2)R_{\phi_{p1}}(\beta_1)\rho_x R_{\phi_{p1}}^\dagger(\beta_1)I_x R_{\phi_{p2}}^\dagger(\beta_2)$ is just a similarity transform of $R_{\phi_{p1}}(\beta_1)\rho_x R_{\phi_{p1}}^\dagger(\beta_1)I_x$ under which the trace is invariant. A commutation $[R_{\phi_{p2}}(\beta_2), I_x] = 0$ can be avoided by setting $\phi_{p2} \neq n\pi$. For $M_y(\phi_{p2}, \beta_2, \phi_{p1}, \beta_1)$ a commutator $[R_{\phi_{p2}}(\beta_2), I_y] = 0$ is avoided for $\phi_p \neq (2n+1)\frac{\pi}{2}$. These constraints on the parameters of type phase ϕ_p implement the functions $M_x(\phi_{p2}, \beta_2, \phi_{p1}, \beta_1)$ such as those shown in Table 5 and Figure 6: these examples were deliberately chosen such that the two fixed variables are taken as having equal values of $\frac{\pi}{2}$.

One can see that class 0, 1 and 3 gates can be implemented by all possible permutations of fixed pairs of variables of identical value (here $\frac{\pi}{2}$). The non-commutation constraint provides the non-canalising behaviour of class 3 gates, while the inherent periodicity of the system is sufficient to provide the canalising input configurations necessary for class 0 and 1 gates. However, periodicity does not suffice for a class 2 gate implementation. Comparing the single-pulse scenario (Figure 4(a)) with the contour plots in Figure 6

	ϕ_{p2}	β_2	ϕ_{p1}	β_1	$M_x(\phi_{p2}, \beta_2, \phi_{p1}, \beta_1)$
(a)	A	$\frac{\pi}{2}$	B	$\frac{\pi}{2}$	$\frac{\lambda_B}{4} (\cos \phi_{p2} \cos \phi_{p1} \cos(\phi_{p2} - \phi_{p1}) - \sin \phi_{p2} \sin \phi_{p1})$
(b)	A	$\frac{\pi}{2}$	$\frac{\pi}{2}$	B	$\frac{\lambda_B}{4} (\cos^2 \phi_{p2} \cos \beta_1 - \sin \phi_{p2} \sin \beta_1)$
(c)	$\frac{\pi}{2}$	A	$\frac{\pi}{2}$	B	$\frac{\lambda_B}{4} \cos(\beta_2 + \beta_1)$
(d)	$\frac{\pi}{2}$	A	B	$\frac{\pi}{2}$	$\frac{\lambda_B}{4} (\cos^2 \phi_{p1} \cos \beta_2 - \sin \phi_{p1} \sin \beta_2)$
(e)	A	B	$\frac{\pi}{2}$	$\frac{\pi}{2}$	$-\frac{\lambda_B}{4} \sin \phi_{p2} \sin \beta_2$
(f)	$\frac{\pi}{2}$	$\frac{\pi}{2}$	A	B	$-\frac{\lambda_B}{4} \sin \phi_{p1} \sin \beta_1$

TABLE 5

Examples of logic gate implementations from $M_x(\phi_{p2}, \beta_2, \phi_{p1}, \beta_1)$ using any possible pair of variables as gate input A and B , and fixing the remaining two parameters to $\frac{\pi}{2}$. Apart from a change in sign, examples (e) and (f) are identical to the case in Figure 4(a). Example (d) is identical to (b).

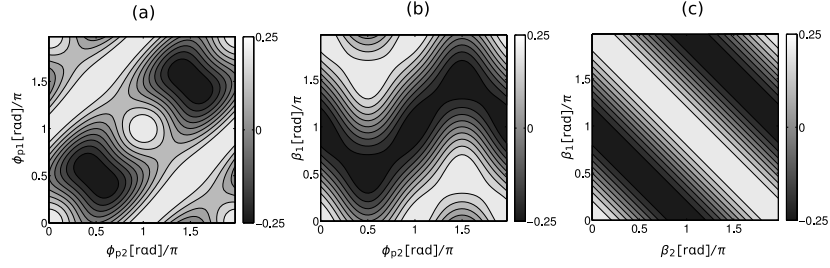


FIGURE 6

Contour plots of $M_x(\phi_{p2}, \beta_2, \phi_{p1}, \beta_1)$ corresponding to examples (a)–(c) in Table 5.

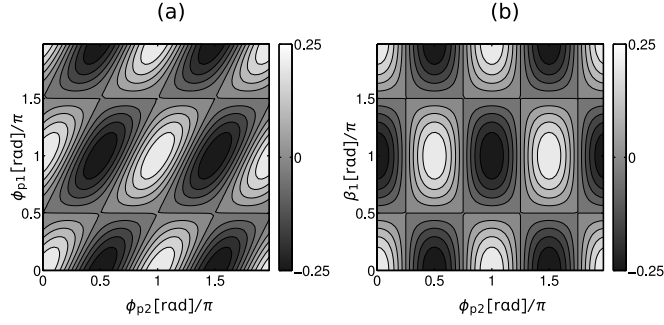


FIGURE 7
Contour plot of $M_x(\phi_{p2}, \beta_2, \phi_{p1}, \beta_1)$ for (a) $\beta_1 = \frac{\pi}{2}$, $\beta_2 = \pi$ and for (b) $\phi_{p1} = \frac{\pi}{2}$, $\beta_2 = \pi$.

demonstrates that class 2 gate implementations require horizontal and vertical traces of constant value zero. Such traces are absent in the contour plots in Figure 6. In short, arbitrarily choosing pairs of fixed parameters as equal valued (not just for $\frac{\pi}{2}$) leads to the loss of universality.

Let us examine if universality is regained if the fixed parameters are no longer taken as equal valued. For example, taking $\beta_1 = \frac{\pi}{2}$ and $\beta_2 = \pi$ gives $M_x(\phi_{p2}, \beta_2, \phi_{p1}, \beta_1) = \frac{\lambda_B}{4} \cos(2\phi_{p2} - \phi_{p1}) \cos(\phi_{p1})$. The corresponding contour plot is shown in Figure 7(a) highlighting the presence of constant horizontal zero-valued traces. Allowing for unequal-valued pairs of parameters β_1 and β_2 (or ϕ_{p1} and ϕ_{p2}) permits implementation of class 0, 1 and 2 gates but not class 3.

Universality is regained if pairs of parameters of *different types*, e.g. ϕ_{p1} and β_2 are fixed and do *not* assume equal values. Figure 7(b) shows that $\phi_{p1} = \frac{\pi}{2}$, $\beta_2 = \pi$ gives $M_x(\phi_{p2}, \beta_2, \phi_{p1}, \beta_1) = \frac{\lambda_B}{4} \cos 2\phi_{p2} \cos \beta_1$. Both horizontal and vertical zero-valued traces are re-established in the corresponding contour plot (Figure 7(b)); all 2-input logic gates can be obtained.

The flexibility and the ease of implementation as seen from our illustrative examples are good indicators for the richness of the natural computational potential of this system. Computational operations more complicated than just 2-input boolean logics are therefore well within the grasp of this system. This includes multi-input logic gates, continuous logic, and analogue computing implementations. The ubiquitous occurrence of function values $\{-1, 0, 1\}$, due to the trigonometric system functions, especially holds promise for the

implementation of a balanced ternary logic as being natural to this particular system [7]. Note also, that we can reverse the operation of a logic gate if we know the pulse(s) that originally generated the output [20]. This does not match with the usual predictions about a computation where e.g. NAND gates are not reversible [8]. Obviously our raw output stores additional information that can be exploited for more sophisticated computations.

4 SUMMARY AND CONCLUSIONS

We have provided a design approach to analysing novel substrates in order to determine which of their parameters can be used to implement boolean logic gates. We have illustrated this with a case study drawn from NMR-based classical computation. The design process requires cataloguing the parameters that are naturally used to describe and manipulate the target system, analysing their behaviours in combinations, and then matching the resulting patterns of behaviour with the corresponding behaviour patterns of the target gate classes. Our case study here focusses on two particular parameters ($\beta = \kappa_p \tau_p$ and ϕ_p); a full design study would assess other combinations of other parameters, since the aim is not simply to find *some* solution, but to analyse the ‘natural’ computational capabilities of the substrate. For example, in our work on continuous gates [6], we focussed on ω_p and τ_p .

The design approach is not restricted to 2-input gates; combining several parameters can produce patterns corresponding to more complex gates. More sophisticated experiments could directly exploit symmetry properties of the Hamiltonian (Eq. (11)–(14)). Eventually, however, specific behaviours will be more easily achieved by combining simpler gates in circuits than by directly designing complex gates.

Circuit design requires additional analysis to determine how individual gates can be combined in a circuit in a manner ‘natural’ for the substrate in question. Circuit design requires determining techniques for: sequencing parameter manipulations to implement the sequence of gate operations in a circuit; combining manipulations to implement multiple gate operations in parallel; routing and transforming the output of one gate to the appropriate input of the next. We will address these circuit design issues in a companion paper [5].

This work addresses only how to implement ‘classical’ boolean logic gates in unconventional substrates, yet it is clear that the example system has further information available, that is thrown away when viewing it as a boolean gate. If this extra information is instead retained and exploited, more powerful

computation becomes available [1]. The real computational power of these novel substrates will come from not viewing them as merely alternative ways of implementing classical logic gates, but from exploiting them to implement non-classical forms of computation: quantum, continuous (analogue), hybrid, and more. The design approach described here forms a first step in a principled approach for analysing substrates with a view to performing a specified form of computation.

5 ACKNOWLEDGEMENTS

Support of this work by the Deutsche Forschungsgemeinschaft and Leverhulme grant FM/00224/AM is gratefully acknowledged. We thank Alastair Abbott for constructive comments.

REFERENCES

- [1] Alastair A. Abbott, Matthias Bechmann, Christian S. Calude, and Angelika Sebald. (May 2011). A nuclear magnetic resonance implementation of a classical Deutsch-Jozsa algorithm. submitted.
- [2] Andrew Adamatzky. (2007). Physarum machines: encapsulating reaction-diffusion to compute spanning tree. *Naturwissenschaften*, 94(12):975–980.
- [3] Leonard M. Adleman. (1994). Molecular computation of solutions to combinatorial problems. *Science*, 266(5187):1021–1024.
- [4] Martyn Amos. (2005). *Theoretical and Experimental DNA Computation*. Springer.
- [5] Matthias Bechmann, Angelika Sebald, and Susan Stepney. Direct wiring of multi-gate NMR logic circuits. In preparation.
- [6] Matthias Bechmann, Angelika Sebald, and Susan Stepney. (2010). From binary to continuous gates—and back again. In *ICES 2010, York, UK, September 2010*, volume 6274 of *LNCS*, pages 335–347. Springer.
- [7] Matthias Bechmann, Angelika Sebald, and Susan Stepney. (2011). Design of ternary logic gates: a nuclear magnetic resonance case study. In preparation.
- [8] Charles H. Bennett. (1982). The thermodynamics of computation—a review. *Int. J. Theor. Phys.*, 21:905–940.
- [9] Vinícius P. Correia, André I. Reis, Cep Porto, and Alegre Rs Brasil. (2001). Classifying n-input boolean functions. In *Proc. VII Workshop de Iberchip, IWS, Montevideo*, page 58.
- [10] Barbara Drossel. (2009). *Random Boolean Networks*, pages 69–110. Wiley.
- [11] Solomon Golomb. (1959). On the classification of boolean functions. *IRE Transactions on Information Theory*, 5(5):176–186.
- [12] Simon L. Harding and Julian F. Miller. (2004). A tone discriminator in liquid crystal. In *CEC 2004*, pages 1800–1807. IEEE Press.
- [13] Simon L. Harding and Julian F. Miller. (2005). Evolution in materio: A real-time robot controller in liquid crystal. In *Proc. NASA/DoD Conference on Evolvable Hardware*, pages 229–238. IEEE Press.

- [14] Simon L. Harding, Julian F. Miller, and Edward A Rietman. (2008). Evolution in materio: Exploiting the physics of materials for computation. *Int. J. Unconventional Computing*, 4(2):155–194.
- [15] Yorik Hardy and Willi H. Steeb. (2001). *Classical and Quantum Computing*. Birkhäuser Verlag, Basel.
- [16] Jonathan A. Jones. (2001). NMR quantum computation. *Prog. Nucl. Magn. Reson. Spectrosc.*, 38(4):325–360.
- [17] Jonathan A. Jones. (2011). Quantum computing with nmr. *Progress in Nuclear Magnetic Resonance Spectroscopy*, 59(2):91–120.
- [18] Viv Kendon, Angelika Sebald, Susan Stepney, Matthias Bechmann, Peter Hines, and Robert C. Wagner. (2011). Heterotic computing. In *Unconventional Computation 2011*, number 6714 in LNCS, pages 113–124. Springer.
- [19] Lothar Kuhnert, Konstantin Agladze, and Valentin Krinsky. (1989). Image processing using light-sensitive chemical waves. *Nature*, 337:244–247.
- [20] Malcolm. H. Levitt. (April 2008). *Spin Dynamics: Basics of nuclear magnetic resonance*. John Wiley & Sons, Ltd, Chichester, 2nd edition.
- [21] Jonathan W. Mills. (2008). The nature of the extended analog computer. *Phys. D*, 237(9):1235–1256.
- [22] Jonathan W. Mills, Matt Parker, Bryce Himebaugh, Craig Shue, Brian Kopecky, and Chris Weilemann. (2006). “Empty Space” computes: The evolution of an unconventional supercomputer. In *Proc. of the 3rd conference on Computing frontiers*, pages 115–126.
- [23] Ikuko N. Motoike and Andrew Adamatzky. (2005). Three-valued logic gates in reaction-diffusion excitable media. *Chaos, Solitons & Fractals*, 24(1):107–114.
- [24] Marta Roselló-Merino, Matthias Bechmann, Angelika Sebald, and Susan Stepney. (2010). Classical computing in nuclear magnetic resonance. *Int. J. Unconventional Computing*, 6(3–4):163–195.
- [25] Jun J. Sakurai. (1994). *Modern Quantum Mechanics*. Addison-Wesley Publishing Company, Reading, MA, Revised edition.
- [26] Benjamin Schumacher. (Apr 1995). Quantum coding. *Phys. Rev. A*, 51(4):2738–2747.
- [27] Jakub Siewewiesiuk and Jerzy Gorecki. (2001). Logical functions of a cross-junction of excitable chemical media. *J. Phys. Chem. A*, 105(35):8189–8195.
- [28] David Slepian. (1953). On the number of symmetry types of boolean functions of n variables. *Can. J. Math.*, 5(2):185–193.
- [29] Susan Stepney. (July 2008). The neglected pillar of material computation. *Physica D*, 237(9):1157–1164.
- [30] Susan Stepney, Samson Abramsky, Andy Adamatzky, Colin Johnson, and Jon Timmis. (2008). Grand challenge 7: Journeys in non-classical computation. In *Visions of Computer Science*, pages 407–421. BCS.
- [31] Atsushi Tero, Seiji Takagi, Tetsu Saigusa, Kentaro Ito, Dan P. Bebber, Mark D. Fricker, Kenji Yumiki, Ryo Kobayashi, and Toshiyuki Nakagaki. (2010). Rules for biologically inspired adaptive network design. *Science*, 327(5964):43–442.
- [32] Ágota Tóth and Kenneth Showalter. (1995). Logic gates in excitable media. *J. Chem. Phys.*, 103:2058–2066.
- [33] Damien Woods and Thomas J. Naughton. (2008). Parallel and sequential optical computing. In *Optical SuperComputing*, volume 5172 of LNCS, pages 70–86. Springer.

- [34] Damien Woods and Thomas J. Naughton. (2009). Optical computing. *Appl. Math. Comput.*, 215(4):1417–1430.
- [35] Stephen S. Yau and Calvin K. Tang. (feb. 1970). Universal logic modules and their applications. *IEEE Transactions on Computers*, C-19(2):141–149.